Nonlinear Compton scattering with a laser pulse

Madalina Boca* and Viorica Florescu
Department of Physics and Centre for Advanced Quantum Physics, University of Bucharest, MG-11, Bucharest-Măgurele 077125, Romania

(Received 10 August 2009; published 5 November 2009)

We investigate the scattering of intense laser radiation on free electrons using a semiclassical relativistic approach. The laser field is described as an ideal pulse with a finite duration, a fixed direction of propagation, and indefinitely extended in the plane perpendicular to it. This allows the use of Volkov solutions and leads to a transition amplitude which is a product of a three-dimensional delta function with a linear combination of three one-dimensional integrals that we evaluate numerically. We give the general expression of the emitted photon spectrum as a function of frequency and direction valid for any initial geometry of the electron-laser beam scattering and for arbitrary shape, duration, and polarization of the laser pulse averaged over the initial electron spin and summed over the emitted photon and ejected electron polarizations. At a fixed photon scattering angle, one obtains a continuous frequency distribution with a succession of maxima located near the discrete values corresponding to the monochromatic case. We present results for head-on collisions and circularly polarized laser pulses. Our figures illustrate the dependence of the photon spectrum on pulse parameters (duration, shape, and maximum intensity) and the role of the initial electron energy. For a few-cycle linearly polarized pulse we also explore the effect of the carrier-envelope phase.

DOI: 10.1103/PhysRevA.80.053403 PACS number(s): 32.80.Wr, 12.20.Ds

I. INTRODUCTION

Low intensity electromagnetic radiation scattering on free electrons, the usual Compton scattering, is explained by the interaction of an electron with a single photon. The interest in the modifications of the process in the case *of an intense radiation beam*, expressed in several papers published soon after the laser was invented, has been almost constantly present in the literature since. A recent paper [1] by Ehlotzky *et al.* gives details on the main moments in the evolution of the theoretical studies and on the experimental progress on this and other related processes. An extensive bibliography is also contained in an even more recent paper [2] devoted to the theoretical quantitative description of the effect in the case of the head-on collision of a circularly polarized monochromatic plane wave with an energetic electron.

The name attached to the process in which a photon is emitted as a result of the interaction of an electron with an intense electromagnetic radiation field is *nonlinear Compton scattering*. The process is named sometimes harmonic generation, especially when the classical description is adopted [3] or nonlinear Thomson scattering [4] in the nonrelativistic regime (low energy electrons, low laser frequency). The relationship between the Thomson and Compton scattering in the high intensity regime was considered by Gao [5]. In the case of an electromagnetic *monochromatic* plane wave, the semiclassical theory, based on a classical description of the laser field and a quantum description of the photon emission, supports the possibility of describing the process as the simultaneous absorption of a number of photons N, with the integer N, taking any positive value. As a consequence, at a fixed detection direction, the emitted photon spectrum contains more than one frequency. The name laser Compton scattering is used especially when the contribution from $N=1$ is investigated being practically the only one detectable; strong field effects, as the frequency shift with respect to the Compton line, are nevertheless less studied in this case, the experimental interest being oriented toward the possibility of building x-ray sources with remarkable performances in terms of monochromaticity and polarization [6].

The first experimental detection of nonlinear Compton scattering, due to Englert and Rinehart [7], is the observation of the second harmonic ($N=2$) working with electrons in the keV range and with a Q-switched Nd:YAG laser. In the experiment performed at SLAC [8], using 46.6 GeV electrons and terawatt pulses from a Nd:glass laser at 1054 and 527 nm wavelengths, the scattered electrons were detected and the measured signal was interpreted as due to the contribution of up to $N=4$ photons. In the experiment [9] performed at Brookhaven National Laboratory, Accelerator Test Facility (BNL-ATF), using a 60 MeV electron beam and a CO_2 laser with the wavelength of 10.6 μm, the photon spectrum was investigated for energies lower than 6.5 keV. Agreement with the calculations based on semiclassical theory was found. Another recent experiment [10] reports the detection of the second harmonics using a low energy electron beam (10 keV) and an intense laser with the peak intensity of 4×10^{15} W/cm^2, but disagreement with theory.

The usual treatment of laser assisted or induced processes is the semiclassical description mentioned before in which the external electromagnetic field is treated classically but the atomic system is described within the frame of quantum mechanics and, if spontaneous photon emission takes place, as in Compton scattering, or (e^+,e^-), pairs are created, the electron interacts also with the quantized electromagnetic field. In the case of an electron in the field of a monochromatic electromagnetic plane wave, the emitted frequency spectrum is discrete, its lines being dependent on the detection direction characterized by the unity vector $\mathbf{n}'$, according to the equation [1,11,12]

*boca@barutu.fizica.unibuc.ro

$$\omega'_N = \frac{N\omega(E_1 - c\mathbf{p}_1\cdot\mathbf{n})}{E_1 - c\mathbf{p}_1\cdot\mathbf{n}' + (N\hbar\omega + \tilde{U}_P)(1-\mathbf{n}\cdot\mathbf{n}')}, \quad N = 1,2,\ldots, \tag{1}$$

where ω is the frequency of the external field propagating in the direction of the unity vector $\mathbf{n}$, $\mathbf{p}_1$, and E_1, the initial electron momentum and energy, m, the electron mass, c, the velocity of the light and

$$\tilde{U}_P = \frac{mc^2}{E_1 - c\mathbf{p}_1\cdot\mathbf{n}}U_P, \quad U_P = \frac{a_L^2}{4}mc^2,$$

$$a_L^2 = \frac{8\pi r_0}{mc\omega^2}I. \tag{2}$$

Here r_0 is the electron classical radius and I is the radiation intensity. The quantity denoted by U_P is the ponderomotive energy of the electron in the field and it is proportional to the laser intensity. Frequency spectrum (1) follows from the conservation laws of the total four momentum for the interaction of the electron with N, quanta associated with the external field leading to a scattered electron and an emitted photon, in which laser dressed energies and momenta are used for the electron [24]. For $N=1$, and weak fields $a_L^2 \ll 1$, the frequency reduces to that of the Compton line. The expression of the photon distribution for a circularly polarized monochromatic electromagnetic wave can be found even in textbooks [13].

The parameter a_L, defined in Eq. (2), dependent on both intensity and frequency, and independent of the Planck constant, is used to characterize different regimes for the external field. The value of a_L for the experiment [8] at SLAC is of the order of 1. The regime $a_L \gg 1$ is reached at high intensities and low frequencies.

The main calculations on the nonlinear Compton effect, based on the semiclassical formalism and modeling the external electromagnetic field by a *monochromatic* plane wave, besides the first ones [11,12], are those published by Ehlotzky and co-workers through the years, part of them presented in their review paper [1]. Comparisons between results based on Klein-Gordon and Dirac equations reveal cases in which spin effects matter. The paper [2] adds new and systematic results to the monochromatic case. The photon spectra for several values of a parameter connected with the intensity are depicted in a movielike sequence of plots. For other details on the literature and previous calculations of Compton effect the two papers [1,2] are recommended.

For the monochromatic case there are many calculations in which the electron interaction with the field is treated classically [3,14–17]. A unique analytic result is due to Goreslavski *et al.* [16] who have obtained, by a direct analytic calculation, a closed form for the photon angular distribution corresponding to any initial configuration of the electron and laser beams. They have reobtained the same result as the classical limit of the quantum expression, which is a series for which the summation cannot be performed analytically.

Only a few papers have gone beyond the monochromatic case and the majority of them are calculations based on classical electromagnetism. We quote only the most recent ones [18,19].

Our paper goes beyond the monochromatic case describing the intense external electromagnetic field as *a radiation pulse*. The calculation is done in *semiclassical relativistic theory*. The same formalism was adopted by Narozhnyi and Fofanov [20] for a circularly polarized laser pulse. During the analytic calculation they made approximations justified for the case of very long pulses; we shall refer to these while presenting our method in Sec. III. Narozhnyi and Fofanov have then calculated the photon spectral angular distribution for the case of head-on collision of an ultrarelativistic electron with a laser field with frequency $\omega=1.17$ eV and a_L equal to 1, 1.5, and 2, an intensity range in which only the first few harmonics of the laser effectively appear in the spectrum. They have noticed details of the structure of the peaks that they can explain using their analysis based on the stationary phase approximation. When working in the conditions adopted by Narozhnyi and Fofanov, our calculations confirm their observations and numerical results.

In Sec. II we briefly go through the formalism leading to the general formulas (14) and (15) of the transition amplitude for nonlinear Compton scattering in terms of Volkov solutions expressed as a four-dimensional integral. In the monochromatic case this integral is a series of products of four δ functions. In the case of a laser pulse, by a convenient choice of the variables, only three of the four integrals can be performed analytically and, as shown in Sec. III, the amplitude is reduced to form (18) in which three δ functions appear, multiplying a factor containing three one-dimensional integrals [Eq. (25)]. Their evaluation is all that is needed in the numerical calculation. Although one of these integrals is divergent, we argue that it can be written as the sum of a term that does not contribute and a convergent integral. Then in Sec. IV we write the expressions of the relevant cross sections.

Our numerical results are presented in Sec. V. First, we define the "effective" pulse duration, denoted by $\tilde{\tau}_p$, that we use in order to calculate the transition rate of the nonlinear Compton effect. Then we present spectral-angular distributions for the frequency $\omega=0.043$ a.u. and very high field intensity (maximum intensity during the pulse of the order of 10^{19} W/cm^2). We consider two situations: (i) the initial electron at rest and (ii) the initial ultrarelativistic electron counterpropagating with the intense pulse. For the very intense laser field, many harmonics (up to $N\sim 100$) contribute to the spectrum and the corresponding peaks are broad and overlap; on the other hand, in the case of relatively low intensity, only the first few harmonics are visible and the individual peaks are well defined, their shape depending on the shape of the laser pulse. Next, we show that for very short pulses it is possible to detect the signature of the absolute phase of the laser pulse in the spectral angular distribution. Finally, we discuss the nonrelativistic limit and the retardation effects on the photon spectrum.

Appendixes A and B contain general equations implied by the formalism. Appendix C describes the situation of the divergent integral we meet. Finally, in Appendix D we refer to the monochromatic case and we give details on how this limit follows from our equations.

II. BRIEF REVIEW OF THE QUANTUM DESCRIPTION OF NONLINEAR COMPTON SCATTERING

The semiclassical formalism we adopt is identical to that used before [11,12], i.e., a hybrid theory in which the electron interacts with an external electromagnetic field described classically by a four-vector potential **A**, and with the quantized electromagnetic field A_c, written as in Eq. (A1). Laser Compton scattering is identified with the spontaneous emission of a photon by an electron interacting with the external field.

In our work the laser pulse is modeled as an electromagnetic field that propagates in a fixed direction, characterized by the unity vector **n**, has a finite extension in the direction of propagation, but extends to infinity in the plane perpendicular to this direction. We use a fixed reference system with the z axis along **n**. Such a field is described by a vector potential **A**, orthogonal to **n**, and depending only on the variable

$$\phi = t - z/c. \tag{3}$$

In the following we shall use the four vectors

$$n = (1,\mathbf{n}), \quad \tilde{n} = (1,-\mathbf{n}), \quad n^2 = \tilde{n}^2 = 0, \quad n\cdot\tilde{n} = 2. \tag{4}$$

Then one has $\phi = n\cdot x/c$, where x is the position four-vector. The shape of $\mathbf{A}(\phi)$ will come into play later, as in the absence of the quantized field, the Dirac equation admits exact solutions for any $\mathbf{A}(\phi)$. These solutions, named Volkov solutions, are reproduced in Appendix B. We shall assume that the vector potential decreases rapidly and is practically zero outside of a finite range of the variable.

In the hybrid approach described before, the Dirac Hamiltonian is

$$H = c\boldsymbol{\alpha}\cdot[\mathbf{P} - e\mathbf{A}(\phi) - e\mathbf{A}_c(x)] + e\Phi_c(x) + mc^2\beta + H_{0,c}, \tag{5}$$

where $e<0$ is the electron charge, **P**, the momentum operator, $H_{0,c}$ is the Hamiltonian of the free electromagnetic quantized field and $\boldsymbol{\alpha}$ and β are the usual Dirac matrices. In the following we use the γ matrices

$$\gamma_0 = \beta, \quad \boldsymbol{\gamma} = \beta\boldsymbol{\alpha}, \tag{6}$$

which have the property $\gamma_\mu^\dagger = \gamma_0\gamma_\mu\gamma_0$, $\mu = 0,\ldots,3$. Using them in the Hamiltonian, the term corresponding to the interaction with the quantized electromagnetic field is

$$H_{\text{int}} = ec\gamma^0\hat{A}_c, \quad \hat{A}_c \equiv \frac{\Phi_c}{c}\gamma_0 - \mathbf{A}_c\cdot\boldsymbol{\gamma} \tag{7}$$

and is treated as a weak perturbation. All the remaining terms represent the "free" system consisting of the electron in the laser field and the quantized electromagnetic field without interaction. The evolution operator for this system is denoted by U_0.

The initial and final states are

$$|\Psi_1(-\infty)\rangle = \frac{1}{\sqrt{V}}|\xi_{i_1}(p_1)\rangle\exp\left(\frac{i}{\hbar}\mathbf{p}_1\cdot\mathbf{r}\right)\otimes|0\rangle, \tag{8}$$

$$|\Psi_2(\infty)\rangle = \frac{1}{\sqrt{V}}|\xi_{i_2}(p_2)\rangle\exp\left(\frac{i}{\hbar}\mathbf{p}_2\cdot\mathbf{r}\right)\otimes|1_{k_2,s_2}\rangle, \tag{9}$$

where in each state the first factor is a free electronic solution of the Dirac equation with fixed momentum and spin; the spinor $|\xi_i(p)\rangle$ is a solution of Eq. (B5). The symbols $|0\rangle$ and $|1_{k_2,s_2}\rangle$ denote the vacuum and one-photon Fock state, respectively.

In the transition amplitude

$$\mathcal{M}_{1\to2} = \langle\Psi_2(\infty)|U(\infty,-\infty)|\Psi_1(-\infty)\rangle, \tag{10}$$

with U, the evolution operator of the whole system, we treat in the first order of perturbation theory the interaction of the electron with the quantized electromagnetic field, which is responsible for the photon emission, and we use the action of the free evolution operator U_0, on the initial and final states, leading to the Volkov states $|\psi_i(p;x)\rangle$ defined in Eq. (B4),

$$U_0(t,-\infty)|\Psi_1(-\infty)\rangle = |\psi_{i_1}(p_1;x)\rangle\otimes|0\rangle \equiv |\Psi_1(t)\rangle, \tag{11}$$

$$\langle\Psi_2(\infty)|U_0(\infty,t) = \langle\psi_{i_2}(p_2;x)|\otimes\langle 1_{k_2,s_2}| \equiv \langle\Psi_2(t)|. \tag{12}$$

Thus, we obtain

$$\mathcal{M}_{1\to2} = \frac{ec}{i\hbar}\int_{-\infty}^{\infty} dt\langle\Psi_2(t)|\gamma^0\hat{A}_c|\Psi_1(t)\rangle. \tag{13}$$

After replacing the initial and final states and the expression of the quantized field (A1) in the transition amplitude, one obtains

$$\mathcal{M}_{1\to2} = \frac{ec}{i\hbar}\sqrt{\frac{\hbar}{2\epsilon_0\omega_2 V}}\mathcal{T}_{1\to2} \tag{14}$$

with

$$\mathcal{T}_{1\to2} = \int_{-\infty}^{\infty} dt\langle\bar{\psi}_{i_2}(p_2;x)|\hat{s}_2\exp(ik_2\cdot x)|\psi_{i_1}(p_1;x)\rangle, \tag{15}$$

where we have used the notations $\langle\bar{\psi}| = \langle\psi|\gamma^0$ and $\hat{s}_2 = s_2\cdot\gamma = (s_2)^0\gamma_0 - \mathbf{s}_2\cdot\boldsymbol{\gamma}$. The subscripts 2 and 1 correspond to the final and initial states characterized by the four-momentum p_2 and p_1, respectively, and by the spin index i_2 and i_1, respectively. We shall use real polarization four vectors s_2.

III. ONE-PHOTON TRANSITION AMPLITUDE BETWEEN TWO VOLKOV SOLUTIONS IN THE CASE OF A LASER PULSE

A. General structure of the matrix $\mathcal{T}_{1\to2}$

We describe here the quantity $\mathcal{T}_{1\to2}$, defined in Eq. (15), which is proportional to the transition amplitude, as was shown at the end of the previous section. In more detail, using expressions (B4) of the two Volkov solutions, with notations explained in Appendix B, the function we have to evaluate is a quadruple integral over the variables **r**, and t,

$$\mathcal{T}_{1\to 2}=\frac{1}{V}\int_{-\infty}^{\infty}dt\int d\mathbf{r}\langle\bar{\xi}_{i_2}(p_2)|\bar{\Omega}_{i_2}(p_2;\phi)\hat{s}_2\Omega_{i_1}(p_1;\phi)\times|\xi_{i_1}(p_1)\rangle\exp\left\{-\frac{i}{\hbar}[x\cdot(p_1-p_2-\hbar k_2)+F(p_1;\phi)-F(p_2;\phi)]\right\},\tag{16}$$

where the function $F(p;\phi)\equiv F_1(p;\phi)$, with F_1, defined in Eq. (B7) with the sign factor $\epsilon_1=1$. Defining the new variables of integration $\mathbf{r}_\perp$ (the position in the plane perpendicular to the propagation direction) $\phi=t-z/c$, and $\tilde{\phi}=t+z/c$, and using the property

$$x\cdot(p_1-p_2-\hbar k_2)=\frac{c}{2}\tilde{\phi}n\cdot(p_1-p_2-\hbar k_2)+\frac{c}{2}\phi\tilde{n}\cdot(p_1-p_2-\hbar k_2)-\mathbf{r}_\perp\cdot(\mathbf{p}_{1\perp}-\mathbf{p}_{2\perp}-\hbar\mathbf{k}_{2\perp}),\tag{17}$$

one can directly perform the integrals over $\mathbf{r}_\perp$ and $\tilde{\phi}$ obtaining three one-dimensional δ functions,

$$\mathcal{T}_{1\to 2}=I_{\mathbf{A}}(2,1)\frac{(2\pi\hbar)^3}{V}\delta(\mathbf{p}_{1\perp}-\mathbf{p}_{2\perp}-\hbar\mathbf{k}_{2\perp})\times\delta[n\cdot(p_1-p_2-\hbar k_2)],\tag{18}$$

where

$$I_{\mathbf{A}}(2,1)=\int_{-\infty}^{\infty}d\phi Q_{21}(\phi)\exp\left\{-\frac{i}{\hbar}\left[\frac{c}{2}\phi\tilde{n}\cdot(p_1-p_2-\hbar k_2)+F(p_1;\phi)-F(p_2;\phi)\right]\right\}\tag{19}$$

and

$$Q_{21}(\phi)\equiv\langle\bar{\xi}_{i_2}(p_2)|\bar{\Omega}_{i_2}(p_2;\phi)\hat{s}_2\Omega_{i_1}(p_1;\phi)|\xi_{i_1}(p_1)\rangle.\tag{20}$$

B. Simplified form of matrix elements Q_{21}

In the algebraic calculations implied by the summation over the spins of the incident and scattered electrons, a particular choice of the polarization four vector s_2 is suitable [12]. Starting from any polarization four vector s_2 (orthogonal on k_2 and of norm -1), one builds another polarization vector

$$\tilde{s}_2=s_2-\frac{s_2\cdot k_1}{k_1\cdot k_2}k_2\tag{21}$$

whose properties are

$$\tilde{s}_2\cdot\tilde{s}_2=s_2\cdot s_2=-1,\quad \tilde{s}_2\cdot k_2=s_2\cdot k_2=0,\quad \tilde{s}_2\cdot k_1=0,\tag{22}$$

i.e., this new polarization four vector is orthogonal on *both* k_1 and k_2. In our calculation k_1 is proportional to n defined in Eq. (4). In the following we shall assume that such a choice was made, and, by direct calculation one obtains easily

$$Q_{21}(\phi)=\langle\bar{\xi}_{i_2}(p_2)|\hat{s}_2|\xi_{i_1}(p_1)\rangle-\frac{e}{2n\cdot p_1}\langle\bar{\xi}_{i_2}(p_2)|\hat{s}_2\hat{A}(\phi)\hat{n}|\xi_{i_1}(p_1)\rangle-\frac{e}{2n\cdot p_2}\langle\bar{\xi}_{i_2}(p_2)|\hat{n}\hat{A}(\phi)\hat{s}_2|\xi_{i_1}(p_1)\rangle.\tag{23}$$

Next we shall define two new four vectors

$$n_x\equiv(0,\mathbf{e}_x),\quad n_y=(0,\mathbf{e}_y),\qquad n_x\cdot n_y=0,\quad n_x\cdot n_x=n_y\cdot n_y=-1,\tag{24}$$

where $\mathbf{e}_x$ and $\mathbf{e}_y$ are the unity vectors of the x axis and y axis, respectively, of the reference system and we introduce the integrals

$$\mathcal{B}(2,1)\equiv\int_{-\infty}^{\infty}d\phi\exp\left\{-\frac{i}{\hbar}\left[\frac{c}{2}\phi\tilde{n}\cdot(p_1-p_2-\hbar k_2)+F(p_1;\phi)-F(p_2;\phi)\right]\right\},\tag{25}$$

$$\mathbf{A}(2,1)\equiv-\int_{-\infty}^{\infty}d\phi\frac{e\mathbf{A}(\phi)}{mc}\exp\left\{-\frac{i}{\hbar}\left[\frac{c}{2}\phi\tilde{n}\cdot(p_1-p_2-\hbar k_2)+F(p_1;\phi)-F(p_2;\phi)\right]\right\}.\tag{26}$$

With Eqs. (18), (19), and (23), the final expression of transition amplitude (14) becomes

$$\mathcal{M}_{1\to 2}=-iec\sqrt{\frac{1}{2\epsilon_0\omega_2\hbar}}\frac{(2\pi\hbar)^3}{V^{3/2}}\delta(\mathbf{p}_{1,\perp}-\mathbf{p}_{2,\perp}-\hbar\mathbf{k}_{2,\perp})\delta(n\cdot(p_1-p_2-\hbar k_2))\mathcal{Q}(2,1),\tag{27}$$

where

$$\mathcal{Q}(2,1)=\left\{\mathcal{B}(2,1)\langle\bar{\xi}_{i_2}(p_2)|\hat{s}_2|\xi_{i_1}(p_1)\rangle+(mc)\mathcal{A}_x(2,1)\times\left[\frac{1}{2(n\cdot p_2)}\langle\bar{\xi}_{i_2}(p_2)|\hat{n}\hat{n}_x\hat{s}_2|\xi_{i_1}(p_1)\rangle+\frac{1}{2(n\cdot p_1)}\langle\bar{\xi}_{i_2}(p_2)|\hat{s}_2\hat{n}_x\hat{n}|\xi_{i_1}(p_1)\rangle\right]+(mc)\mathcal{A}_y(2,1)\times\left[\frac{1}{2(n\cdot p_2)}\langle\bar{\xi}_{i_2}(p_2)|\hat{n}\hat{n}_y\hat{s}_2|\xi_{i_1}(p_1)\rangle+\frac{1}{2(n\cdot p_1)}\langle\bar{\xi}_{i_2}(p_2)|\hat{s}_2\hat{n}_y\hat{n}|\xi_{i_1}(p_1)\rangle\right]\right\}\tag{28}$$

and $\mathcal{A}_x(2,1)$ and $\mathcal{A}_y(2,1)$ are the two Cartesian components of the integral $\mathbf{A}(2,1)$ defined in Eq. (26).

Up to now we did not specify the explicit form of the external electromagnetic pulse described by the vector potential $\mathbf{A}$. In the following we shall consider the case

$$\mathbf{A}(\phi) = A_0 f(\phi)[\mathbf{e}_x \cos(\zeta/2)\cos(\omega\phi) - \mathbf{e}_y \sin(\zeta/2)\sin(\omega\phi)]. \tag{29}$$

The laser polarization is described by the parameter ζ ($\zeta=0$ and π correspond to linear polarization, $\zeta=\pm\pi/2$, to circular polarization) and the unity vectors $\mathbf{e}_x$ and $\mathbf{e}_y$ are chosen along the axes of the ellipse associated with the state of polarization. In the *monochromatic case* $f=1$ and ω is the laser frequency. In the case of a *laser pulse* the function f is the pulse envelope. This function is significantly different from zero only in a finite interval $(\phi_{\text{in}}, \phi_{\text{f}})$. The maximum amplitude reached by the electric field of the pulse is ωA_0.

Before going further, we show precisely the differences between our approach and that of Narozhnyi and Fofanov [20] who have made approximations valid only in the case $\omega\tau \gg 1$, where the parameter τ is a measure of the pulse duration: they start with an approximation of the exponential factor in the Volkov solution (B4), as in their Eq. (8), and continue with a Fourier expansion over an interval $[\phi, \phi+2\pi]$, for the integrand of the integral which represents the transition amplitude for which they take then a zeroth-order approximation in $1/\omega\tau$. We work with analytic expressions (27) and (28) without making further approximations. Some remarks on the integrals $\mathcal{B}$ and $\mathcal{A}$ are necessary and we continue with them before we describe the next operations that lead to the cross sections.

C. Properties of the integrals $\mathcal{B}(2,1)$, and $\mathcal{A}(2,1)$

In the *monochromatic case* the integrands of the integrals $\mathcal{B}(2,1)$ and $\mathbf{A}(2,1)$ in Eqs. (25) and (26) are periodic functions of ϕ and so is the function $\mathcal{Q}(2,1)$ in Eq. (28). This allows each integral to be expanded in a Fourier series and each term is found to be proportional to a one-dimensional δ function. The coefficients depend on the laser intensity and polarization. They are proportional to Bessel functions for circular polarization, which represents the simplest situation. For illustration, such an expansion is given in Appendix D for the case of the integral $\mathcal{B}$.

Here we work with these integrals for the case of a *finite pulse*. Due to the presence of the vector potential in front of the exponential in the integrand of $\mathbf{A}$, this integral has finite limits ϕ_{in} and ϕ_{f}. This is not the case of the integral $\mathcal{B}(2,1)$ for which the integrand does not vanish at $-\infty$ or ∞. The situation is complicated by the fact that the behavior of the integrand is different at the two limits. We discuss this integral in Appendix C and we justify that what is needed for the evaluation of the probability of the process is the convergent integral

$$\tilde{\mathcal{B}}(2,1) = \frac{2}{\tilde{n}\cdot(\hbar k_2 + p_2 - p_1)} \int_{\phi_{\text{in}}}^{\phi_{\text{f}}} \left[\frac{1}{2}\left(\frac{1}{n\cdot p_1} - \frac{1}{n\cdot p_2}\right) e^2 \mathbf{A}^2(\phi) - e\mathbf{A}(\phi)\cdot\left(\frac{\mathbf{p}_1}{n\cdot p_1} - \frac{\mathbf{p}_2}{n\cdot p_2}\right)\right] \exp\left\{ -\frac{i}{\hbar}\left[\frac{c}{2}\phi\tilde{n}\cdot(p_1 - p_2 - \hbar k_2) + F(p_1;\phi) - F(p_2;\phi)\right]\right\} d\phi. \tag{30}$$

IV. NONLINEAR COMPTON SCATTERING CROSS SECTIONS

We define a transition rate by dividing the probability of photon emission and simultaneous electron scattering by a quantity $\tilde{\tau}_p$, which is meant to be an effective duration of the laser pulse,

$$d^{(4)}\Gamma_{1\to 2} = \frac{|\mathcal{M}_{1\to 2}|^2}{\tilde{\tau}_p} \frac{V d\mathbf{k}_2}{(2\pi)^3} \frac{V d\mathbf{p}_2}{(2\pi\hbar)^3}. \tag{31}$$

For some pulse shapes the definition of $\tilde{\tau}_p$ appears to be a matter of convention. In Sec. V we shall give the definition of this quantity for the pulses we use in our calculation.

The square of the δ functions in the transition rate is treated by the usual procedure,

$$\delta^2(\mathbf{p}_{1\perp} - \mathbf{p}_{2\perp} - \hbar\mathbf{k}_{2\perp})\delta^2(n\cdot(p_1 - p_2 - \hbar k_2)) = \delta(\mathbf{p}_{1\perp} - \mathbf{p}_{2\perp} - \hbar\mathbf{k}_{2\perp})\delta(n\cdot(p_1 - p_2 - \hbar k_2))\frac{V}{(2\pi\hbar)^3}. \tag{32}$$

The differential cross section is obtained by dividing the above rate by the relative average flux of the ingoing electrons and photons. In the case of a monochromatic laser field its expression is [21]

$$J = \frac{\epsilon_0 \omega A_0^2}{2\hbar}\frac{n\cdot p_1}{m}. \tag{33}$$

In the monochromatic case and for weak fields the cross section obtained this way reduces to the linear Compton effect cross section. We use the same expression for the case of a laser pulse with a finite duration described by vector potential (29); in this case, A_0 will be the amplitude of the vector potential $\mathbf{A}$ at the pulse peak intensity and ω the central frequency of the pulse. However, this is a matter of choice just as is the use of the effective duration $\tilde{\tau}_p$.

A. Most differential cross section

Using the previous results, the most differential cross section corresponding to the situation in which the initial electron spin is fixed and both final electron spin and emitted photon polarization are detected is

$$d^{(4)}\sigma^{\text{pol}} = r_0^2 \frac{2}{\pi}\frac{c^3}{\tilde{\tau}_p}\frac{(mc)^2}{(eA_0)^2}\frac{mc}{n\cdot p_1}\frac{|\mathcal{Q}(2,1)|^2}{\omega\omega_2}\delta(\mathbf{p}_{1\perp} - \mathbf{p}_{2\perp} - \hbar\mathbf{k}_{2\perp})\delta(n\cdot(p_1 - p_2 - \hbar k_2))d\mathbf{k}_2 d\mathbf{p}_2. \tag{34}$$

In order to get the cross section for unpolarized initial electrons and no final electron polarization detection, we use relation (A2), with the result

$$\frac{1}{2}\sum_{\text{spins}} |\mathcal{Q}(2,1)|^2 = \frac{1}{2(p_1)^0(p_2)^0}\Big[|\tilde{\mathcal{B}}|^2[2(p_2\cdot s_2)(p_1\cdot s_2) + (p_1\cdot p_2) - (mc)^2] + 2(mc)^2|\mathcal{A}\cdot s_2|^2 - (\mathcal{A}\cdot\mathcal{A}^*)\frac{(mc)^2}{2}\frac{(\hbar k_2\cdot n)^2}{(n\cdot p_1)(n\cdot p_2)}$$

$$+(mc)\mathrm{Re}\left\{\tilde{\mathcal{B}}^*\left\{2(\mathcal{A}\cdot s_2)[s_2\cdot(p_1+p_2)]+\mathcal{A}\cdot(p_1+p_2)-\frac{(p_1\cdot n)}{(p_2\cdot n)}(p_2\cdot\mathcal{A})-\frac{(p_2\cdot n)}{(p_1\cdot n)}(p_1\cdot\mathcal{A})\right\}\right\}\Bigg] \tag{35}$$

where, for the sake of compactness, we have introduced a four vector $\mathbf{A}(2,1)$ attached to the integral $\mathcal{A}(2,1)$ in Eq. (26) defined as $\mathcal{A}(2,1)\equiv(0,\mathbf{A}(2,1))$.

We sum now over the emitted photon polarization using formula (A3) with the result

$$\begin{aligned}\frac{1}{2}\sum_{\mathrm{spins},s_2}|\mathcal{Q}(2,1)|^2&=\frac{1}{2(p_1)^0(p_2)^0}\left\{2|\tilde{\mathcal{B}}|^2\left(\frac{(p_1\cdot k_1)(p_2\cdot k_2)+(p_1\cdot k_2)(p_2\cdot k_1)}{k_1\cdot k_2}-(mc)^2\right)+\left(\frac{(\hbar k_2\cdot n)^2}{(n\cdot p_1)(n\cdot p_2)}+2\right)\left[-(mc)^2(\mathcal{A}\cdot\mathcal{A}^*)\right.\right.\\&\left.\left.+2(mc)\frac{(n\cdot p_1)(n\cdot p_2)}{\hbar k_2\cdot n}\mathrm{Re}\left\{\tilde{\mathcal{B}}^*\left(\frac{\mathcal{A}\cdot p_1}{n\cdot p_1}-\frac{\mathcal{A}\cdot p_2}{n\cdot p_2}\right)\right\}\right]\right\}\\&\equiv\langle|\mathcal{Q}|^2\rangle.\end{aligned} \tag{36}$$

Finally, the differential cross section with unpolarized particles can be written as

$$d^{(4)}\sigma^{\mathrm{unpol}}=r_0^2\sigma^{(4)}\delta(\mathbf{p}_{1\perp}-\mathbf{p}_{2\perp}-\hbar\mathbf{k}_{2\perp})\times\delta(n\cdot(p_1-p_2-\hbar k_2))d\mathbf{k}_2d\mathbf{p}_2, \tag{37}$$

with

$$\sigma^{(4)}\equiv\frac{2}{\pi}\frac{c^3}{\tilde{\tau}_p}\frac{(mc)^2}{(eA_0)^2}\frac{mc}{n\cdot p_1}\frac{\langle|\mathcal{Q}|^2\rangle}{\omega\omega_2}. \tag{38}$$

B. Spectral-angular distribution of the emitted photon

By integrating the most differential cross section (37) over the final electron momentum $\mathbf{p}_2$, one obtains the differential cross section relevant to the case in which only the emitted photon energy and direction are detected. The integral can be analytically calculated using the three δ functions present in the expression of $d^{(4)}\sigma^{\mathrm{unpol}}$. The conservation laws implied by them,

$$n\cdot(p_1-p_2-\hbar k_2)=0,\quad \mathbf{p}_{1\perp}-\mathbf{p}_{2\perp}-\hbar\mathbf{k}_{2\perp}=\mathbf{0}, \tag{39}$$

lead to the solution $\mathbf{p}_2=\tilde{\mathbf{p}}_2$, where

$$\tilde{\mathbf{p}}_{2\perp}=\mathbf{p}_{1\perp}-\hbar\mathbf{k}_{2\perp},\quad \tilde{p}_{2z}=\frac{(mc)^2+\mathbf{p}_{2\perp}^2}{2n\cdot(p_1-\hbar k_2)}-\frac{n\cdot(p_1-\hbar k_2)}{2}. \tag{40}$$

Then the product of the three δ functions becomes up to a factor a 3D δ function,

$$\delta(\mathbf{p}_{1\perp}-\mathbf{p}_{2\perp}-\hbar\mathbf{k}_{2\perp})\delta(n\cdot(p_1-p_2-\hbar k_2))=\frac{(\tilde{p}_2)^0}{n\cdot\tilde{p}_2}\delta(\mathbf{p}_2-\tilde{\mathbf{p}}_2). \tag{41}$$

Using the above results the doubly differential cross section can be written as

$$d^2\sigma_\gamma=r_0^2\left\{\sigma^{(4)}\frac{(\tilde{p}_2)^0}{n\cdot\tilde{p}_2}\right\}_{\mathrm{cons}}d\mathbf{k}_2\equiv r_0^2\sigma^{(2)}(\omega_2,\mathbf{n}')d\omega_2d\Omega_2, \tag{42}$$

where the index "cons" means that everywhere in expression (38) of $\sigma^{(4)}$ the conservation rule (40) must be applied. From here, by integrating over the emitted photon frequency, we can get an angular distribution $d\sigma/d\Omega_2$, or, integrating over the photon direction, a frequency spectrum $d\sigma_\gamma/d\omega_2$.

We mention also *the nonrelativistic limit*. In the dipole approximation, when vector potential (29) is replaced by the function dependent on time only

$$\mathbf{A}(t)=A_0f(t)[\mathbf{e}_x\cos(\zeta/2)\cos(\omega t)-\mathbf{e}_y\sin(\zeta/2)\sin(\omega t)], \tag{43}$$

the most differential cross section has the structure

$$d\sigma_{\mathrm{NR,DA}}^{(4)}=r_0^2\sigma_{\mathrm{NR,DA}}^{(4)}\delta(\mathbf{p}_1-\mathbf{p}_2-\hbar\mathbf{k}_2)d\mathbf{k}_2d\mathbf{p}_2. \tag{44}$$

The main difference between the nonrelativistic and relativistic result (37) comes from the conservation law implied by the δ function. In the nonrelativistic case the sum of the final electron momentum and the emitted photon momentum is equal to the initial electron momentum, while in the relativistic case this is true only for the momenta components orthogonal to the direction of the propagation $\mathbf{n}$ of the laser pulse; for the z components a more complicated Eq. (40) involving also the four vector n has to be satisfied.

By integrating the previous expression over the electron momentum we obtain the photon doubly differential cross section, which will be written as

$$d^2\sigma_{\gamma,\mathrm{NR,DA}}=r_0^2\sigma_{\mathrm{NR,DA}}^{(2)}(\omega_2,\mathbf{n}')d\omega_2d\Omega_2. \tag{45}$$

V. NUMERICAL RESULTS FOR EMITTED PHOTON SPECTRAL AND ANGULAR DISTRIBUTIONS

All the results we present refer to the case of head-on collisions and unpolarized particles. The quantity we have calculated is the photon distribution $\sigma^{(2)}$, defined in Eq. (42), a function of the emitted frequency ω_2, and the emitted photon direction. It has the dimension of time/solid angle and it will be given in atomic units. We pointed out previously that we use a reference system with z axis along the laser propagation direction and x axis along one of the axes of the polarization ellipse of the laser. In the case of circular polarization and head-on collision the z axis is an axis of symmetry. All our graphs will present $\sigma^{(2)}$ as a function of the emitted photon frequency ω_2 with a fixed direction of the emitted photon.

We consider only one laser frequency, $\omega=0.043$ a.u. ≈ 1.17 eV. All the figures, except for Fig. 4, refer to an

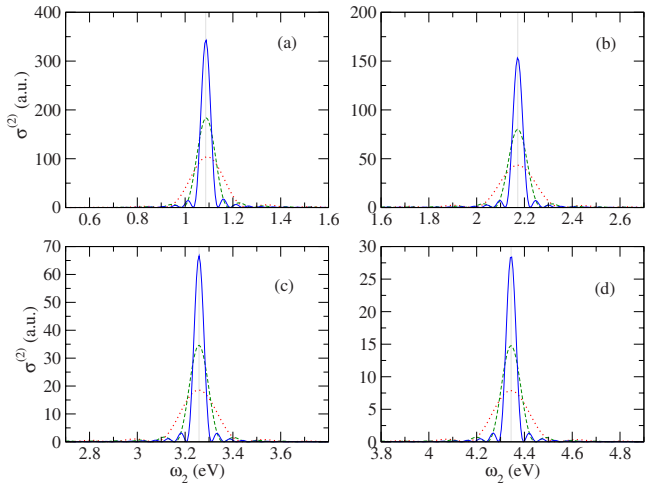

FIG. 1. (Color online) $\sigma^{(2)}$ at $\theta=9°$ for a circularly polarized rectangular pulse with $\eta=5$ and different durations: $\tau_c=5T$, dotted (red) line; $\tau_c=10T$, dashed (green) line; and $\tau_c=20T$ full (blue) line. The initial electron is at rest.

initial electron at rest. The laser pulse intensity is characterized by the parameter $\eta=|e|A_0/(mc)$, where A_0 is the maximum amplitude of the vector potential in Eq. (29); for the case of a monochromatic pulse one has $\eta\equiv a_L$, with a_L, defined in Eq. (2). At the chosen frequency, $\eta=1$ corresponds to a maximum intensity of the pulse of 1.2×10^{18} W/cm^2 and $\omega\tilde{\tau}_p=5$ for an effective pulse duration of 2.8 fs.

Our presentation, which is more exploratory than systematic, is focused on the influence of the pulse duration and shape on the photon emission. In Eq. (31) we have defined the most differential cross section using the "effective duration" of the pulse $\tilde{\tau}_p$. The concrete choice for this parameter will be discussed in what follows.

We start with results for a pulse with very short (less than one cycle) turn-on and turn-off and a relatively long (at least five optical cycles) flat region; in the following we shall name such a pulse a "rectangular" one. In this case the obvious choice for the effective pulse duration $\tilde{\tau}_p$ is the length τ_c of the constant part of the pulse. In Fig. 1 we present $\sigma^{(2)}$ for the case of an electron initially at rest; the laser pulse is circularly polarized, $\eta=5$ (this corresponds to the maximum intensity of 3×10^{19} W/cm^2) and the emitted photon angle is $\theta=9°$ with respect to the initial direction of the laser pulse. Results are given for three values of pulse duration: $\tau_c=5T$ (dotted line), $10T$ (dashed line), and $20T$ (full line), where $T=2\pi/\omega$, is the laser period. The range in which the spectrum is represented, $\omega_2\in(0.5,5)$ eV, is split in four smaller intervals, each of them represented in one of the four plots. One can see that the spectrum consists of well-defined maxima located at the same positions as in the monochromatic limit given by Eq. (1) and marked by gray lines; each plot contains one of the first four maxima. We can attach an integer label N starting from 1 to each peak; when the pulse duration increases the maxima become higher and sharper as expected. The amplitude of the successive peaks decreases rapidly (note the different scales on the ordinate), but their shape, at constant τ_c, is almost independent of N. We have checked that for different values of $\tau_c\geq5T$ the area under each peak, which we shall denote in the following by $\tilde{\sigma}_N^{(2)}$ is practically the same for all the graphs centered on the same frequency ω_N', and it is equal to the value of the monochromatic cross section $\sigma_N^{(2)}$, defined in Eq. (D13), calculated for the same conditions. We have also checked the agreement between $\sigma_N^{(2)}$ and $\tilde{\sigma}_N^{(2)}$ for the case of rectangular pulses with $\tau_c\geq5T$ for all the intensities and scattering geometries presented in our figures. This check is in fact one of the tests of the correctness of our results.

We remark the simplicity of the situation met in the case of the rectangular pulse: the maxima are centered on the position of the lines corresponding to the monochromatic limit, even for very short pulses. The frequency distribution around each peak is always symmetric with respect to the maximum and the peaks have practically no structure.

In the following we consider two pulses for which the constant region of the envelope $f(\phi)$ of vector potential (29) is absent, the pulse consisting only of two "wings," a Gaussian pulse with the envelope

$$f_G(\phi)=\exp(-\phi^2/\tau^2) \tag{46}$$

and the hyperbolic secant pulse

$$f_{\text{sech}}(\phi)=\frac{1}{\cosh(\phi/\tau)}. \tag{47}$$

In both cases it is obvious that the envelope has negligible values except for a finite duration, proportional to the parameter τ, in the expression of the envelope, and, as a consequence, the factor $\tilde{\tau}_p$ (the effective pulse duration) used in Eq. (31) should be chosen as $\tilde{\tau}_p=\lambda\tau$. The choice of the constant factor λ is a matter of convention. We explain our choice in the following. We have found, by calculating $\sigma^{(2)}$ with a fixed arbitrary value of the proportionality constant λ, and different values of τ, that the area under each peak tends to a constant value when τ, increases, as in the case of a rectangular pulse. For a particular case (electron at rest, $\theta=0.01$, circular polarization, $\eta=0.1$ and $N=1$) we have adjusted λ by imposing the condition that the area under the peak corresponding to the limit of very long pulse denoted by $\tilde{\sigma}_1^{(2)}$ takes the value $\sigma_1^{(2)}$ in Eq. (D13). Using this criterion we have obtained for a Gaussian pulse $\lambda_G=0.63$ and for the sech pulse $\lambda_{\text{sech}}=0.98$. We mention here that this choice of the parameter λ ensures in fact very good agreement between $\sigma_N^{(2)}$ and $\tilde{\sigma}_N^{(2)}$ for an initial electron at rest, for any scattering angle, and for a large number of vales of N, in the intensity range $\eta\leq1$. The agreement is poor for higher intensities, but we do not see a reason to expect otherwise.

With the choice made for $\tilde{\tau}_p$, we present results that illustrate the influence of the pulse shape on the spectral distribution. In Fig. 2(a) is represented $\sigma^{(2)}$ in the same conditions as in Fig. 1, i.e., $\eta=5$, circular polarization and the initial electron at rest. The pulse is rectangular in the upper plots, Gaussian in the middle plots, and sech in the lower plots. In the left part of the figure the emission angle of the photon is $\theta=9°$ and to the right $\theta=18°$; the pulse duration is $\omega\tau_c=20\pi$ for the flat pulse, $\omega\tau=30$ for the Gaussian pulse, and $\omega\tau=20$ for the sech pulse.

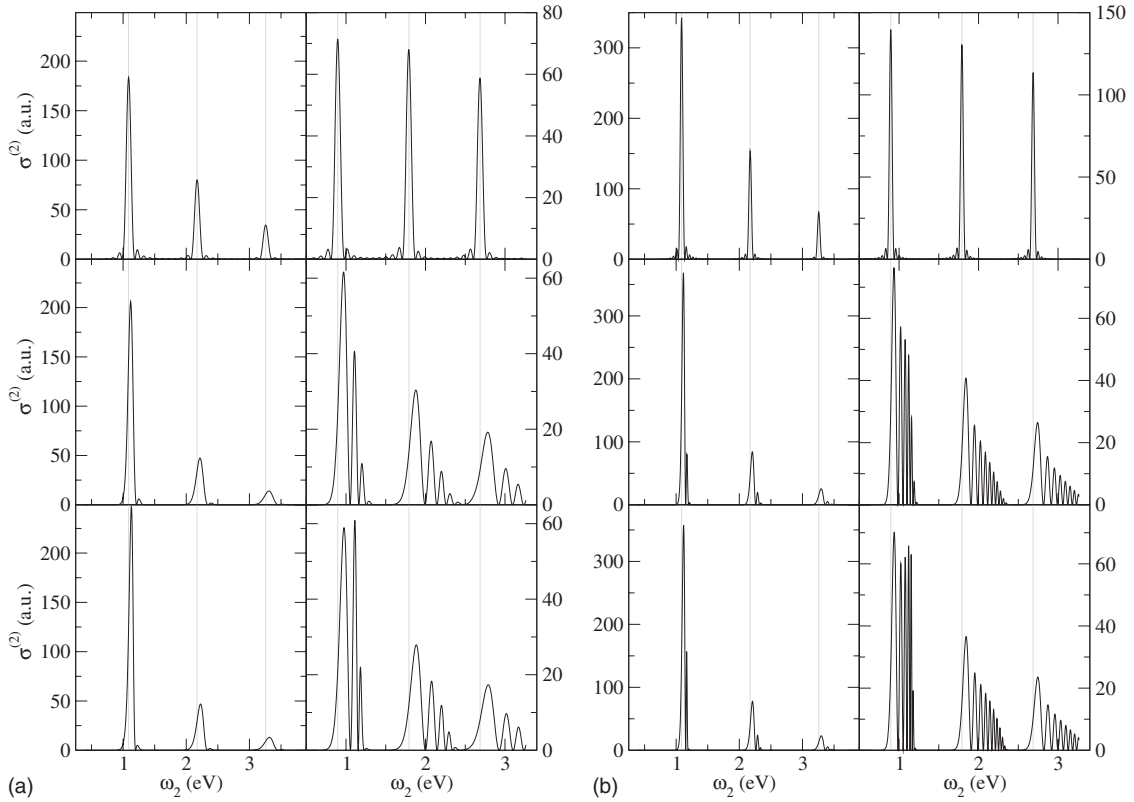

FIG. 2. (a) $\sigma^{(2)}$ for $\eta=5$ and initial electron at rest. Left: $\theta=9°$; right: $\theta=18°$. Rectangular pulse with $\omega\tau_c=20\pi$ (upper plots), Gaussian pulse with $\omega\tau=30$ (middle plots), and sech pulse with $\omega\tau=20$ (lower plot); (b) the same as (a) but $\omega\tau_c=40\pi$ (rectangular pulse, upper plots), $\omega\tau=75$ (Gaussian pulse, middle plots), and $\omega\tau=50$ (sech pulse, lower plots).

Figure 2(b) corresponds to identical conditions as Fig. 2(a), but longer pulses: $\omega\tau_c=40\pi$ for the flat pulse, $\omega\tau=75$ for the Gaussian pulse, and $\omega\tau=50$ for the sech pulse. One can see, as already remarked in Fig. 1, that in all cases the peaks obtained for a rectangular pulse have no structure and become sharper and higher when the pulse duration increases. By contrast, the Gaussian and sech pulses lead to wider peaks with structures which become richer when the scattering angle or the pulse duration increases. A general feature for all cases presented (different pulse shapes and durations) is the much faster decrease in the successive maxima in the spectrum for $\theta=9°$ than for $\theta=18°$.

In the figures presented up to now the successive peaks have a relatively fast decrease with the order N. In order to cover a larger domain of emitted frequencies ω_2, we have evaluated the angular distribution $d\sigma/d\Omega_2$, in the monochromatic case and have found that it has a maximum at $\theta=27°$. Then, for this angle, and for a Gaussian pulse with $\omega\tau=30$, we have represented $\sigma^{(2)}$ in Fig. 3(a). The range of the frequency we have chosen, $\omega_2\leq 70$ eV, contains the first 100 maxima. The inset presents in more detail the interval $\omega_2 \leq 10$ eV and, for comparison, we have represented also the spectrum for a rectangular pulse with $\tau_c=10T$. As in the previous figures, for the rectangular pulse the maxima are very sharp and regular and are located at the corresponding positions of the lines in the monochromatic case marked with gray lines. For the Gaussian pulse, in the region $\omega_2 \leq 10$ eV the peaks have wide structures such that they overlap; the peaks of high order ($N\geq 50$) have lower amplitude and less structure, still their width is of the same order of magnitude as the distance between them and their positions do not coincide with the lines obtained in the monochromatic case.

In Fig. 3(b) we present the same type of situation, now for $\eta=15$ [an intensity nine times larger than in Fig. 3(a)]; the value of the scattering angle, $\theta=9°$, was found using the same criterion as in the previous case. For this intensity the decrease in the amplitude of the peaks is slower but their variation is less monotonic than in the previous case. Also, in the frequency range $\omega_2\leq 10$ eV, the spectrum for a Gaussian pulse is even more irregular than in the case $\eta=5$.

A situation discussed in the literature is that of an initial electron with very high energy; it is convenient in this case to introduce the dimensionless parameter $\gamma=E_{p_1}/mc^2$. If $\gamma \gg 1$ and η is of the order of unity, the angular distribution of the emitted photon $d\sigma/d\Omega_2$ is very sharp, being confined within a cone with the angle of the order of $1/\gamma$, around the initial electron direction [8], and the emitted photon has very large energy. In Fig. 4(a) we present results for the case studied before by Narozhnyi and Fofanov [20]: the initial electron with $\gamma=10^5$ (this value corresponds to the initial energy $E_{p_1}=51.1$ GeV) propagates in the opposite direction with a circularly polarized laser pulse with frequency $\omega=0.043$ and $\eta=1$, the photon being emitted at an angle $\theta_{\gamma-e}=1/\gamma$, with respect to the initial electron direction, i.e., $\theta=\pi-1/\gamma$. We have considered again the two laser pulses, sech (left plots) and Gaussian (right plots); for the sech pulse we have chosen $\omega\tau=50$ (upper plots), 100 (middle plots),

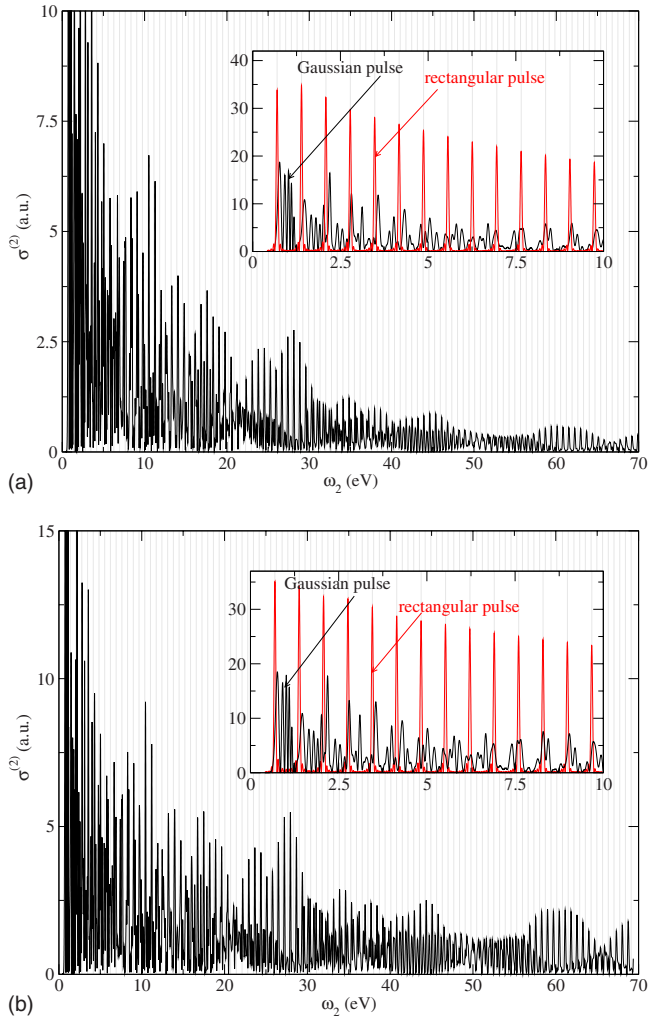

FIG. 3. (Color online) (a) $\sigma^{(2)}$ at $\theta=27°$ for a Gaussian pulse with $\omega\tau=30$, $\eta=5$. Inset: the Gaussian pulse (black line) and a rectangular pulse with $\omega\tau_c=20\pi$ (red line). (b) The same as (a) but at $\theta=9°$ and $\eta=15$. The initial electron is at rest.

and 200 (lower plots); for the Gaussian case the lengths are $\omega\tau=75$, 150, and 300. The spectrum peaks have a very rich structure consisting of oscillations which become faster when the pulse length increases; the envelope of these oscillations is almost independent of the pulse length but changes with the pulse shape. This envelope of the peaks appears to be a characteristic of the pulse shape. The structure of each peak is more blueshifted than redshifted. Narozhny and Fofanov have determined approximate expressions for the left-hand and right-hand limits of each peak. Our numerical calculation confirms their predictions. The mentioned authors did not show the details of the structure of the peaks as they made averages over a small range of frequencies, having in mind a particular value for the resolution of a spectrometer.

In Fig. 4(b) the photon spectral distribution $\sigma^{(2)}$ is represented in the same conditions as in Fig. 4(a) but for a smaller angle $\theta_{\gamma-e}=1/(2\gamma)$. Now the peaks are wider, but the characteristic shape of the first peak, dependent on the pulse envelope, is unchanged. The amplitudes of the higher order peaks compared with that of the first peak are smaller than in the case (a); this property is in agreement with the results we have obtained in the monochromatic case (not reproduced here).

We conclude the discussion of Fig. 4 by emphasizing that it illustrates clearly the behavior of the frequency spectrum with the increase in the pulse duration: the structure of the peaks extends to a finite energy region which practically does not change with the increase in τ; only the number of oscillations and the values of the maxima increase. At a given intensity and emitted photon angle, the peak has a characteristic envelope and the area under it has a well defined limit.

Next, we shall refer to the case of very short pulses containing about 15 or less oscillations of the carrier; we consider a laser field linearly polarized and we allow the carrier-envelope phase (CEP) α_0 to change. The vector potential describing this situation has the form

$$\mathbf{A}(\phi) = \mathbf{e}_x A_0 f(\phi)\sin(\omega\phi + \alpha_0). \tag{48}$$

We can expect that, if the pulse is relatively long and many oscillations of the electromagnetic field are contained in the pulse, the value of the phase α_0 does not influence the results; on the other hand, if we have a very short pulse, α_0 can significantly change the results. Several studies on the effect of the CEP have been done in the case of the ionization of an atom in the laser field [22].

In order to illustrate the effect of the phase, we present in Fig. 5 the values of $\sigma^{(2)}$, for a sech pulse, and two values of CEP: $\alpha_0=-\pi/2$ (left plots) and $\alpha_0=\pi/2$ (right plots). The laser frequency is $\omega=0.043$ a.u. and the maximum intensity is 3×10^{19} W/cm^2 ($\eta=5$); the range of the emitted frequency chosen ($\omega_2\leq1.6$ keV) corresponds in the monochromatic limit to $N\leq230$. The initial electron is at rest and the polar angles of the direction of observation of the emitted photon are $\theta=27°$ and $\phi=0$. We have chosen four durations of the pulse marked on the graphs: $\omega\tau=4,6,8,20$. Note that due to the very fast oscillations one cannot distinguish between the successive peaks. For the shortest pulse the effect of α_0 is noticeable: for $\alpha_0=-\pi/2$, a first region ($\omega_2\leq0.025$ keV) consisting of very fast oscillations of relatively high amplitude is followed by a region where $\sigma^{(2)}$ is very small. By contrast, in the case $\alpha_0=\pi/2$, the first region is shorter and it is followed by two smooth and very broad maxima. When the pulse duration increases, the effect of the relative phase becomes progressively smaller: for $\alpha_0=-\pi/2$ the second maximum increases and moves toward lower frequencies, while for $\alpha_0=\pi/2$ the smooth curves are replaced by a series of very fast oscillations. In the plots corresponding to $\omega\tau=20$ the thick line represents the values of $\sigma^{(2)}$ averaged over intervals of 2.72 eV magnitude. Although at $\omega\tau=20$ the function $\sigma^{(2)}$ presents a series of irregular oscillations with different "shape" for the two values of α_0, one can see that the averaged values are practically identical in the two cases.

Finally, we discuss the nonrelativistic limit of laser-induced Compton scattering. The relevant equations are Eqs. (44) and (45). By comparing the structure of nonrelativistic results [Eq. (44)] with the corresponding relativistic expressions [Eq. (37)] one notices that the main difference is the absence of the laser photon momentum from the conserva-

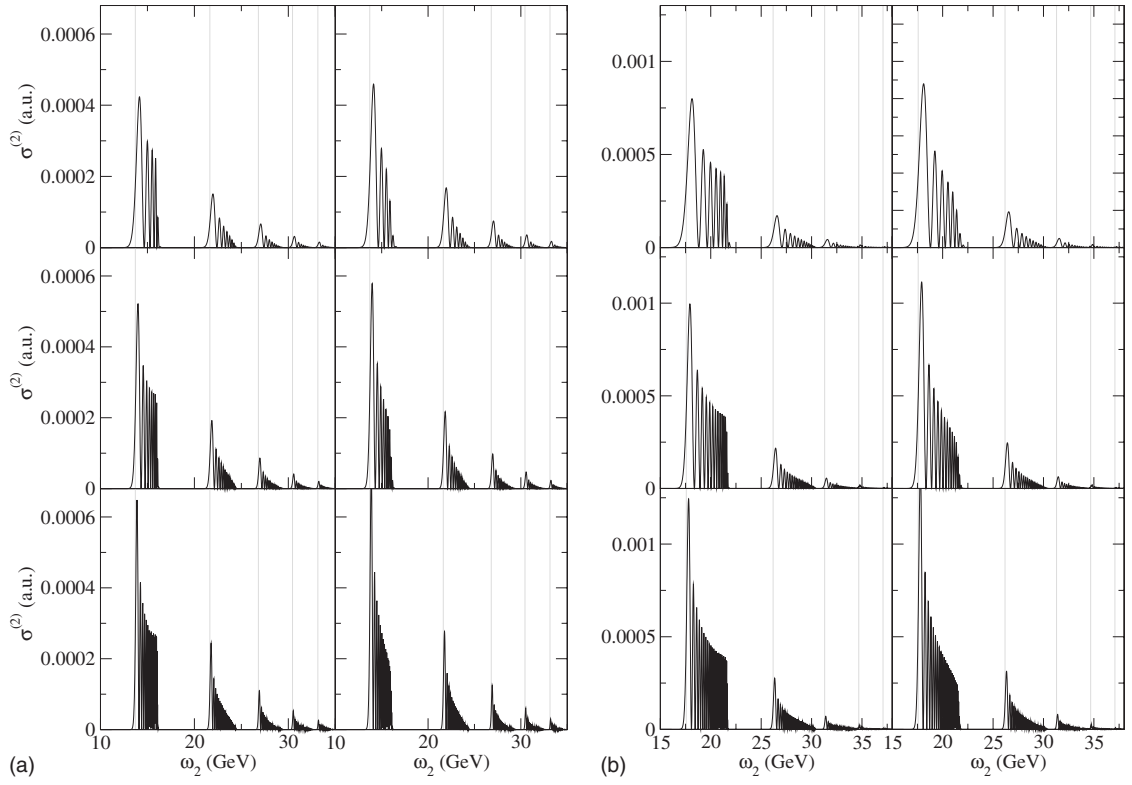

FIG. 4. $\sigma^{(2)}$ for head-on collision, $\gamma=10^5$, $\eta=1$; (a) $\theta_{\gamma-e}=1/\gamma$; left: sech pulse with $\omega\tau=50$ (upper plot), 100 (middle plot), and 200 (lower plot); right: Gaussian pulse with $\omega\tau=75,150,300$. (b) The same as (a) but $\theta_{\gamma-e}=1/(2\gamma)$.

tion rules in the former, which is in fact a consequence of the dipole approximation. Due also to the dipole approximation, if the laser is circularly polarized, the spectral angular distribution $\sigma^{(2)}$ is always perfectly symmetric with respect to the laser polarization plane. In order to give an idea of the relativistic and retardation effects we have chosen a circularly polarized sech pulse with $\omega\tau=10$ and the case of an initial electron at rest. The function $\sigma^{(2)}$ is represented in Fig. 6 for four intensities corresponding to $\eta=2$ (a), 1 (b), 0.5 (c), and 0.1 (d), and in each case for two values of the emitted photon angle, $\theta=36°\equiv\theta_1$ and $\theta=144°\equiv\theta_2$. The nonrelativistic results are represented with full lines; since the two directions are symmetric with respect to the laser polarization plane, the corresponding nonrelativistic results are identical so only one curve is present. The relativistic results for $\theta=\theta_1$ are drawn with dashed lines and those for $\theta=\theta_2$ with dotted lines. One can see that for the highest intensity there is a strong asymmetry between the two directions, which is a measure of the retardation effects. The values for the smaller angle $\theta=\theta_1$ are in all cases closer to the nonrelativistic limit. As the field intensity decreases the relativistic results reduce to the nonrelativistic limit, as should be expected. For $\eta<0.5$, practically only the first peak is visible; for $\eta=0.1$, we have checked that the area under the peak agrees with the value given by the well known Thomson formula, $d\sigma_T/d\Omega=r_0^2(1+\cos^2\theta)/2$.

VI. CONCLUSIONS

In our work we have explored within the semiclassical approach the nonlinear Compton scattering for an electron

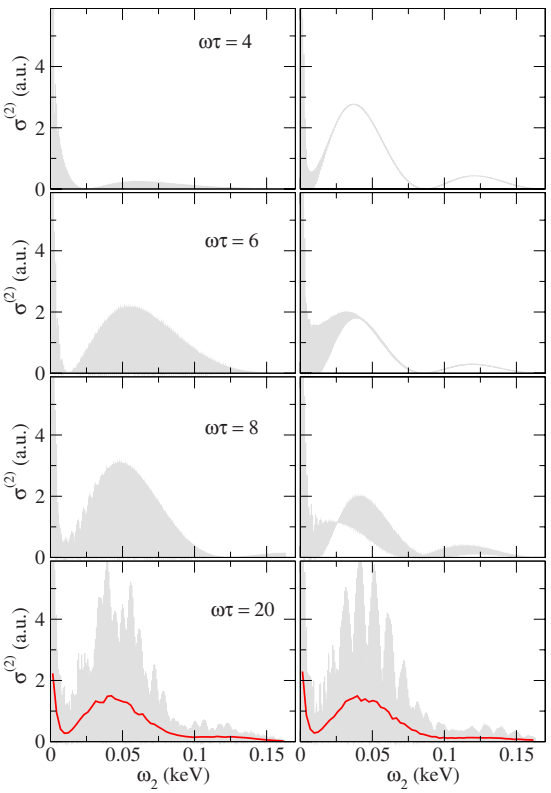

FIG. 5. (Color online) $\sigma^{(2)}$ for laser field (48), $\eta=5$, initial electron at rest, $\theta=27°$, $\phi=0$, and $\omega\tau=4,6,8,20$. Left plots: $\alpha_0=-\pi/2$; right plots: $\alpha_0=\pi/2$. The thick (red) line shows $\sigma^{(2)}$ averaged over intervals of 2.72 eV magnitude.

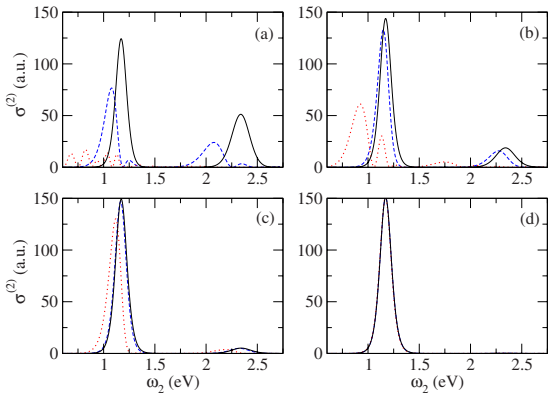

FIG. 6. (Color online) $\sigma^{(2)}$ for a sech pulse with $\omega\tau=10$, and $\eta=2$ (a), $\eta=1$ (b), $\eta=0.5$ (c) and $\eta=0.1$ (d); full (black) line: nonrelativistic results, $\theta=36°$, dashed (blue) line: relativistic results, $\theta=36°$, dotted (red) line: relativistic results, $\theta=144°$.

interacting with a laser pulse indefinitely extended in the plane orthogonal to its fixed direction of propagation. We have derived an analytic expression for the transition amplitude as the product of three δ functions with a linear combination of three one-dimensional integrals that change with the electromagnetic pulse. We then have established the expressions of various cross sections in the case of unpolarized particles. We have evaluated the photon spectrum at fixed photon scattering angle for circularly polarized rectangular, sech, and Gaussian pulses with the frequency of 1.17 eV and different durations. For long pulses, our calculation is in agreement with the results presented by Narozhnyi and Fofanov [20] based on their approximations. For short linearly polarized sech pulses we have illustrated the effect of the absolute phase of the carrier on the spectrum. Finally, we have compared relativistic and nonrelativistic calculations for four pulse intensities.

A more systematic investigation is possible of the spectral-angular distribution $\sigma^{(2)}$ explored here. Also possible is the extension of calculations to the photon spectrum $d\sigma_\gamma/d\omega_2$, or the angular distribution $d\sigma/d\Omega_2$, not studied here, including comparisons with the monochromatic case and with calculations based on classical theory. Our method can be applied to other processes, such as pair creation in a laser field, for which only the monochromatic case was studied.

ACKNOWLEDGMENTS

This work was supported by the Romanian Ministry of Education and Research through Grant No. IDEI-488/2009 for the University of Bucharest. The authors acknowledge Mihai Dondera and Victor Dinu for their comments and useful remarks about the paper. One of the authors (V.F.) is grateful to R. H. Pratt for his hospitality at the University of Pittsburgh, making possible the update of the bibliography.

APPENDIX A: GENERAL EQUATIONS

The quantized electromagnetic field is described by the operators $A_c=(\Phi_c/c,\mathbf{A}_c)$ with the expression

$$A_{c,\mu}(x)=\sum_{n,\lambda}\sqrt{\frac{\hbar}{2\epsilon_0\omega_n V}}[a_{n,\lambda}\exp(-ik_n\cdot x)s_{\lambda,\mu}+a_{n,\lambda}^{\dagger}\exp(ik_n\cdot x)s_{\lambda,\mu}^{*}],\quad x=(ct,\mathbf{r}),\quad \mu=0,\ldots,3. \tag{A1}$$

Here s_λ is the polarization four vector, orthogonal to k_n, and normalized to -1, i.e., $k_n\cdot s_\lambda=0$, $s_\lambda\cdot s_\lambda=-1$. The volume V will disappear from the quantities with physical meaning.

The summation over the electron spins for a 4×4 matrix Λ is expressed by the well-known formula [13]

$$\sum_{i_1,i_2}|\langle\bar{\xi}_{i_2}(p_2)|\Lambda|\xi_{i_1}(p_1)\rangle|^2=\frac{1}{4(p_1)^0(p_2)^0}\mathrm{Tr}\{(\hat{p}_2+mc)\times\Lambda(\hat{p}_1+mc)\bar{\Lambda}\}, \tag{A2}$$

where $\bar{\Lambda}=\gamma^0\Lambda^+\gamma^0$ and the spinors $\xi_j(p)$ are the electronic solutions of Eq. (B5).

The summation over photon polarization in the case of polarization four vectors s_2, orthogonal to the photon momentum k_2, and on another four vector k_1, with $k_1^2=0$, is performed by the formula [11]

$$\sum_{s_2}(A\cdot s_2)(B\cdot s_2)=-A\cdot B+\frac{(A\cdot k_1)(B\cdot k_2)+(A\cdot k_2)(B\cdot k_1)}{k_1\cdot k_2}. \tag{A3}$$

APPENDIX B: VOLKOV SOLUTIONS FOR A LASER PULSE

The Dirac equation for the electron in an external electromagnetic field described by the vector potential $\mathbf{A}$,

$$i\hbar\frac{\partial\psi(x)}{\partial t}=\{c\boldsymbol{\alpha}\cdot[\mathbf{P}-e\mathbf{A}(x)]+mc^2\beta\}\psi(x), \tag{B1}$$

has exact solutions in the case of an arbitrary electromagnetic wave characterized by a fixed direction of propagation $\mathbf{n}$. In this case the potential depends on only one variable

$$\mathbf{A}(x)=\mathbf{A}(\phi),\quad \phi=t-\mathbf{n}\cdot\mathbf{r}/c \tag{B2}$$

and it is orthogonal to $\mathbf{n}$. Using the four vectors

$$A\equiv(0,\mathbf{A}(\phi)),\quad n\equiv(1,\mathbf{n}) \tag{B3}$$

the four solutions associated with the same four vector $p=(E/c,\mathbf{p})$, with $E=\sqrt{m^2c^4+c^2\mathbf{p}^2}$, are

$$\psi_j(p;x)=\frac{1}{\sqrt{V}}\exp\left\{-\frac{i}{\hbar}[\epsilon_j(p\cdot x)+F_j(p;\phi)]\right\}\times\Omega_j(p;\phi)\xi_j(p),\quad j=1,\ldots,4 \tag{B4}$$

where ϵ_j is a sign factor equal to 1 for $j\in\{1,2\}$, and to -1 for $j\in\{3,4\}$, and $\xi_j(p)$ are the solutions of the equation

$$(\hat{p}-\epsilon_j mc)\xi_j(p)=0. \tag{B5}$$

The matrix $\Omega_j(p;\phi)$ is

$$\Omega_j(p;\phi) = I - \frac{\epsilon_j}{2(n\cdot p)} e\hat{A}\hat{n}, \tag{B6}$$

and the function in the exponent is

$$F_j(p;\phi) = \frac{c}{2(n\cdot p)} \int_{\phi_0}^{\phi} d\chi [\epsilon_j e^2 \mathbf{A}^2(\chi) - 2e\mathbf{A}(\chi)\cdot \mathbf{p}_\perp]. \tag{B7}$$

In the case of a pulse, where the vector potential is different from 0 for $\phi \in (\phi_{\text{in}}, \phi_{\text{f}})$, one has $\phi_0 = \phi_{\text{in}}$. In the monochromatic case the indefinite integral can be used, as the choice of an arbitrary value for ϕ_0 leads only to the modification of a phase factor in the Volkov solution.

In the nonrelativistic limit and in the dipole approximation, when the vector potential becomes a function of time only and $p \ll mc$, the Volkov solutions become

$$\psi_{\text{NR,DA}}(\mathbf{p};\mathbf{r},t) = \frac{1}{\sqrt{V}} \exp\left\{\frac{i}{\hbar}\mathbf{p}\cdot[\mathbf{r} - \boldsymbol{\alpha}(t)]\right\} \times \exp\left\{-\frac{i}{\hbar}\left[\frac{\mathbf{p}^2}{2m}t + W(t)\right]\right\} \tag{B8}$$

with

$$\boldsymbol{\alpha}(t) = -\frac{e}{m}\int_{t_0}^{t} dt' \mathbf{A}(t'), \quad W(t) = \int_{t_0}^{t} dt' \frac{e^2\mathbf{A}^2(t')}{2m}. \tag{B9}$$

APPENDIX C: THE INTEGRAL $\mathcal{B}(2,1)$, IN THE CASE OF A LASER PULSE

We write integral (25) as the limit of a convergent integral

$$\mathcal{B}(2,1) = \lim_{\epsilon\to 0} \mathcal{B}_\epsilon(2,1), \tag{C1}$$

where

$$\mathcal{B}_\epsilon(2,1) = \int_{-\infty}^{\infty} b_{21}(\phi) d\phi,$$

$$b_{21}(\phi) = \exp\left\{-\frac{i}{\hbar}[c\tilde{P}\phi + I_{21}(\phi) - \epsilon|\phi|]\right\}. \tag{C2}$$

We have used the notations

$$\tilde{P} = \frac{1}{2}\tilde{n}\cdot(p_1 - p_2 - \hbar k_2), \quad I_{21}(\phi) = F(p_1,\phi) - F(p_2,\phi), \tag{C3}$$

with $F \equiv F_1$, where F_1 is given by Eq. (B7) for $\epsilon_j = 1$. After an integration by parts we obtain

$$\mathcal{B}_\epsilon(2,1) = -\frac{1}{c\tilde{P} - i\epsilon}\int_0^\infty d\phi \frac{dI_{21}(\phi)}{d\phi}\exp\left\{-\frac{i}{\hbar}[(c\tilde{P} - i\epsilon)\phi + I_{21}(\phi)]\right\} - \frac{1}{c\tilde{P} + i\epsilon}\int_{-\infty}^{0} d\phi \frac{dI_{21}(\phi)}{d\phi}\exp\left\{-\frac{i}{\hbar}[(c\tilde{P} + i\epsilon)\phi + I_{21}(\phi)]\right\} - i\hbar \exp\left[-\frac{i}{\hbar}I_{21}(0)\right]\frac{2i\epsilon}{c^2\tilde{P}^2 + \epsilon^2}. \tag{C4}$$

As

$$\frac{dI_{21}(\phi)}{d\phi} = \frac{dF(p_1,\phi)}{d\phi} - \frac{dF(p_2,\phi)}{d\phi} \tag{C5}$$

and using expression (B7) of $F(p,\phi)$, one can see that the first two integrals in Eq. (C4) are convergent in the limit $\epsilon \to 0$, so one can take $\epsilon = 0$, in the first two terms of Eq. (C4); in the last term one recognizes a representation of the Dirac function $\delta(\tilde{P})$. Even more, due to the presence of the factor $\delta(\mathbf{p}_{1,\perp} - \mathbf{p}_{2,\perp} - \hbar\mathbf{k}_{2,\perp})$ $\delta(n\cdot(p_1 - p_2 - \hbar k_2))$ in Eq. (27), the case $\tilde{P} = 0$ never occurs, as the simultaneous equations $n\cdot(p_1 - p_2 - \hbar k_2) = 0$, $\tilde{n}\cdot(p_1 - p_2 - \hbar k_2) = 0$ and $\mathbf{p}_{1\perp} = \mathbf{p}_{2\perp} + \hbar\mathbf{k}_{2\perp}$ are not compatible. Based on the remarks made in this section, we have adopted replacement (30).

APPENDIX D: THE MONOCHROMATIC LIMIT

In the monochromatic case the integrands in $\mathcal{B}(2,1)$ and $\mathcal{A}(2,1)$ are periodic functions of ϕ. The integral F in Eq. (B7) can be done analytically, and we get, for $\epsilon_j = 1$, and after some elementary transformations,

$$F(p_2,\phi) - F(p_1,\phi) = -\frac{ecA_0}{\omega}(\alpha_1 \sin\omega\phi + \alpha_2\cos\omega\phi) + 2\beta_0 U_{\text{P}}\left[\phi + \frac{1}{2\omega}\cos\zeta\sin(2\omega\phi)\right], \tag{D1}$$

where we have defined the dimensionless parameters

$$\alpha_x = \left(\frac{n_x\cdot p_1}{n\cdot p_1} - \frac{n_x\cdot p_2}{n\cdot p_2}\right)\cos\zeta/2,$$

$$\alpha_y = \left(\frac{n_y\cdot p_1}{n\cdot p_1} - \frac{n_y\cdot p_2}{n\cdot p_2}\right)\sin\zeta/2,$$

$$\beta_0 = \frac{mc}{2}\left(\frac{1}{n\cdot p_1} - \frac{1}{n\cdot p_2}\right). \tag{D2}$$

Using the Anger identity

$$e^{-iz\sin\gamma} = \sum_{N=-\infty}^{\infty} J_N(z)e^{-iN\gamma}, \tag{D3}$$

where J_N are Bessel functions of the first kind, the integrand b_{21} of $\mathcal{B}$ can be written as the series

$$b_{21}(\phi) = \exp\left\{ -\frac{i}{\hbar}\left[\frac{\phi}{2}\tilde{n}\cdot(p_1 - p_2 - \hbar k_2) + 2\beta_0 U_P \phi \right] \right\} \sum_N B^{(N)} \exp(iN\omega\phi), \quad \text{(D4)}$$

which leads to the expression of $\mathcal{B}$ as a series of δ functions,

$$\mathcal{B} = \frac{4\pi\hbar}{c} \sum_{N=-\infty}^{\infty} B^{(N)} \delta(\tilde{n}\cdot(q_1 + N\hbar k_1 - q_2 - \hbar k_2)). \quad \text{(D5)}$$

In the previous equation $B^{(N)}$ are some generalized Bessel functions [23]; the initial and final dressed electron four momenta have appeared, with the expressions

$$q_i = p_i + \frac{mU_p}{n\cdot p_i}, \quad i = 1,2. \quad \text{(D6)}$$

The other integral $\mathcal{A}$ can be calculated using the same method and has a similar structure; it follows that the transition amplitude will have the multiphotonic structure

$$\mathcal{M}_{1\to 2}^{\text{monochr}} = \sum_{N=1}^{\infty} M^{(N)} \delta^{(4)}(p_1 + N\hbar k_1 - q_2 - \hbar k_2). \quad \text{(D7)}$$

Note that in the previous equation only the terms with $N \geq 1$ have been included in the sum as the four-dimensional δ function vanishes for $N \leq 0$. The most differential cross section with unpolarized particles becomes

$$d\sigma^{(4)} = r_0^2 \sum_N 2\frac{mc}{n\cdot p_1}\frac{(mc)^2}{e^2 A_0^2}\frac{c^2\hbar}{\omega\omega_2 (p_1)^0 (p_2)^0} \times \mathcal{P}^{(N)} \delta^{(4)}(p_1 + N\hbar k_1 - q_2 - \hbar k_2) d\mathbf{k}_2 d\mathbf{p}_2 \quad \text{(D8)}$$

with

$$\mathcal{P}^{(N)} = -2(mc)^2 |B^{(N)}|^2 + (mc)^2 \left(2 + \frac{\hbar k_2 \cdot n}{(n\cdot p_1)(n\cdot p_2)}\right) \times \left(|A_x^{(N)}|^2 + |A_y^{(N)}|^2 - \frac{e^2 A_0^2}{(mc)^2} \sin^2\zeta/2 |B^{(N)}|^2 \right) - \cos\zeta \, \text{Re}\{B^{(N)} A_{2x}^{(N)*}\}, \quad \text{(D9)}$$

where

$$A_x^{(N)} = \frac{1}{2}(B^{(N-1)} + B^{(N+1)}), \quad \text{(D10)}$$

$$A_y^{(N)} = \frac{1}{2i}(B^{(N-1)} - B^{(N+1)}), \quad \text{(D11)}$$

$$A_{2x}^{(N)} = \frac{1}{4}(B^{(N-2)} + 2B^{(N)} + B^{(N+2)}). \quad \text{(D12)}$$

The previous expression is equivalent to that given by Lyulka [23] in his Eq. (13). As in the case of a finite pulse, by integrating the fully differential cross section over the electron momentum one obtains the doubly differential cross section of the process in which only the photon energy and direction are detected,

$$d^{(2)}\sigma_\gamma = r_0^2 \sum_{N\geq 1} \sigma_N^{(2)} \delta(\omega_2 - \omega_N') d\omega_2 d\Omega_{k_2}. \quad \text{(D13)}$$

This expression still contains δ functions, so, unlike in the case of a laser pulse, for a fixed observation direction the emitted spectrum is discrete, the positions ω_N' of the lines being given by Eq. (1). To each frequency one can attach the value of the function $\sigma_N^{(2)}$ in Eq. (D13).

In the nonrelativistic limit and in dipole approximation the structure of the most differential cross section is

$$d\tilde{\sigma}_{\text{NR,DA}}^{(4)} = r_0^2 \sum_{N\geq 1} \sigma_{N;\text{NR,DA}}^{(4)} p \, \delta(\mathbf{p}_1 - \mathbf{p}_2 - \hbar\mathbf{k}_2) \times \delta\left(\frac{\mathbf{p}_1^2}{2m} + N\hbar\omega - \frac{\mathbf{p}_2^2}{2m} - \hbar\omega_2\right) d\mathbf{k}_2 d\mathbf{p}_2. \quad \text{(D14)}$$

It implies the conservation of nonrelativistic momenta and energy. The laser photon momentum does not appear.

[1] F. Ehlotzky, K. Krajewska, and J. Z. Kaminski, Rep. Prog. Phys. **72**, 046401 (2009).
[2] C. Harvey, T. Heinzl, and A. Ilderton, Phys. Rev. A **79**, 063407 (2009).
[3] E. S. Sarachik and G. T. Schappert, Phys. Rev. D **1**, 2738 (1970).
[4] Y. Y. Lau *et al.*, Phys. Plasmas **10**, 2155 (2003).
[5] J. Gao, Phys. Rev. Lett. **93**, 243001 (2004).
[6] K. Chouffani *et al.*, Adv. X-Ray Anal. **46**, 74 (2003); Laser Part. Beams **24**, 411-419 (2006).
[7] T. J. Englert and E. A. Rinehart, Phys. Rev. A **28**, 1539 (1983).
[8] C. Bula *et al.*, Phys. Rev. Lett. **76**, 3116 (1996); C. Bamber *et al.*, Phys. Rev. D **60**, 092004 (1999).
[9] T. Kumita *et al.*, Laser Phys. **16**, 267 (2006).
[10] M. Iinuma *et al.*, Phys. Lett. A **346**, 255 (2005).
[11] L. S. Brown and T. W. B. Kibble, Phys. Rev. **133**, A705 (1964).
[12] A. I. Nikishov and V. I. Ritus, Zh. Eksp. Teor. Fiz. **46**, 776 (1964) [Sov. Phys. JETP **19**, 529 (1964)]; I. I. Goldman, Phys. Lett. **8**, 103 (1964).
[13] V. B. Berestetskii, E. M. Lifshitz, and L. P. Pitaevskii, *Quantum Electrodynamics*, 2nd ed. (Elsevier, Oxford, 1982).
[14] S. P. Gorelavskii *et al.*, Laser Phys. **2**, 1025 (1992).
[15] Y. I. Salamin and F. H. M. Faisal, Phys. Rev. A **54**, 4383

(1996); **55**, 3964 (1997).
[16] S. P. Gorelavskii, S. V. Popruzhenko, and O. V. Shcherbachev, Laser Phys. **9**, 1039 (1999).
[17] A. Popa, J. Phys. B **41**, 015601 (2008).
[18] G. A. Krafft, Phys. Rev. Lett. **92**, 204802 (2004).
[19] J. Gao, J. Phys. B **39**, 1345 (2006).
[20] N. B. Narozhnyi and M. S. Fofanov, JETP **83**, 14 (1996).
[21] P. Panek, J. Z. Kaminski, and F. Ehlotzky, Opt. Commun. **213**, 121 (2002).
[22] D. B. Milosevic, G. G. Paulus, D. Bauer, and W. Becker, J. Phys. B **39**, R203 (2006).
[23] V. A. Lyulka, Zh. Eksp. Teor. Fiz. **67**, 1638 (1974) [Sov. Phys. JETP **40**, 815 (1975)].
[24] The dressed electron momentum is defined in Appendix D.